Stability and halo formation of a breathing axisymmetric uniform-density beam

Robert L. Gluckstern, Wen-Hao Cheng,* Sergey S. Kurennoy,† and Huanchan Ye‡
Physics Department, University of Maryland, College Park, Maryland 20742
(Received 9 August 1996)

An analysis of the stability and halo formation is presented for a breathing axisymmetric beam of uniform density [Kapchinsky-Vladimirsky (KV) beam] in a uniform focusing channel. Theoretical results are obtained for the form of modes involving nonuniform charge density. In particular, the mismatch-tune depression space is explored, both analytically and by numerical particle-in-cell simulations, to determine the stability limits and growth rates of the most unstable modes. The implications for halo formation are then explored. Halo parameters obtained by simulations are compared with predictions of an analytical model for halo formation from the breathing KV beam developed earlier. The practical applications of the results for high-current linear accelerators are discussed. [S1063-651X(96)05912-0]

PACS number(s): 52.65.Rr, 29.27.Bd, 41.85.−p

I. INTRODUCTION

Interest has arisen recently in using ion linear accelerators in high-current applications, such as the production of tritium, the transformation of radioactive waste to species with shorter lifetimes, and for fission and fusion drivers. Since these applications require average currents in the 100-mA range (100 times larger than that used previously), beam loss must be kept to the order of 1 ppm to avoid serious linear accelerator activation. In particular, it is necessary to understand emittance growth and halo formation in great detail in order to produce an acceptable design.

Accordingly, recent attention has been focused on understanding the mechanism(s) by which halos are produced. This includes a review of observations and related simulations by Jameson [1], a variety of simulations and experiments by Reiser and co-workers [2], and recent simulations by O'Connell *et al.* designed to follow single-particle orbits in a core beam [3]. Several models have been constructed to explore resonances between particle oscillation frequencies and the periodicity of the focusing system or core oscillation modes [4,5]. Many of the simulations show the onset of chaotic motion at high space-charge levels.

In a recent publication [6], we proposed a simple model in which a Kapchinsky-Vladimirsky (KV) beam, excited into a uniform density ''breathing'' mode by some sort of mismatch, interacts resonantly with individual oscillating ions. If the ions find themselves outside the core for part of their oscillation, the resulting nonlinearity of the ion oscillations can lead to a phase lock with the breathing oscillation, producing a halo whose parameters can be predicted and whose appearance matches that in Wangler's simulations [3]. The unanswered question is, What is the mechanism by which ions initially escape from the core in order to participate in the formation of the halo?

Obviously, any unstable longitudinal or transverse collective modes involving the core are capable of moving particles outside the core. Studies of the transverse stability of a matched KV beam [7,8] have shown that instabilities exist for tune depressions (ratio of ion oscillation frequency with space charge to that without space charge) of 0.4 or less. In the present paper, we expand on a previous publication [9] and analyze the instabilities of a breathing KV beam for various collective modes involving nonuniform charge density. We find, not surprisingly, that modes involving a significant breathing amplitude will be unstable at tune depressions as high as 0.7 or 0.8. We then perform multiparticle simulations with a mismatched KV beam for evidence of these unstable modes and the role they play in halo formation.

II. BREATHING MODE

For a KV beam, the motion of an ion within the two-dimensional uniform density beam traveling with axial velocity v_0 is governed by the linear equation

$$\frac{d^2x}{dz^2}+k^2x=\frac{Ix}{a^2}, \tag{2.1}$$

where k is the tune due to the external linear restoring force and I is the perveance defined by

$$I=\frac{eI_0Z_0c}{2\pi Mv_0^3}. \tag{2.2}$$

Here $Z_0=120\pi\ \Omega$ is the impedance of free space, M is the ion mass, c is the speed of light, and I_0 is the beam current. The beam radius a will vary periodically with the axial coordinate z for an azimuthally symmetric breathing beam. We assume that k^2 is independent of z in the present work. An identical equation applies for y for an axisymmetric beam.

The envelope equation corresponding to Eq. (2.1) is

*Present address: Center for Beam Physics, Lawrence Berkeley Laboratory, Berkeley, CA 94720.
†Present address: AOT Division, Los Alamos National Laboratory, Los Alamos, NM 87545.
‡Present address: Advanced Telecommunications Technologies, Inc., Silver Spring, MD 20903.

 © 1996 The American Physical Society

$$a''+k^2a=\frac{I}{a}+\frac{\epsilon^2}{a^3}, \tag{2.3}$$

where the prime stands for d/dz and $\pi\epsilon$ is the transverse emittance of the beam. If we start with $a(0)=a_1$, $a'(0)=0$, an integral of Eq. (2.3) gives

$$a'^2=2I\ \ln\frac{a}{a_1}+k^2(a_1^2-a^2)+\epsilon^2\left(\frac{1}{a_1^2}-\frac{1}{a^2}\right), \tag{2.4}$$

which enables us to obtain the other value of a $(\equiv a_2)$ at which $a'=0$, as well as S, the period of the breathing motion, given by

$$S=2\int_{a_1}^{a_2}\frac{da}{a'(a)}, \tag{2.5}$$

where $a'(a)$ is defined in Eq. (2.4).

We now set $a^2=\beta\epsilon$, where β is in effect the Courant-Snyder amplitude parameter that satisfies

$$\frac{\beta\beta''}{2}+k^2\beta^2=\frac{\beta I}{\epsilon}+1+\frac{\beta'^2}{4}. \tag{2.6}$$

If we now change the independent and dependent variables from z,x,y to

$$\phi=\int\frac{dz}{\beta},\quad u(\phi)=\frac{x(z)}{\sqrt{\beta\epsilon}},\quad v(\phi)=\frac{y(z)}{\sqrt{\beta\epsilon}}, \tag{2.7}$$

we find

$$\ddot{u}+u=0,\quad \ddot{v}+v=0, \tag{2.8}$$

where each dot denotes a derivative with respect to ϕ. Thus the breathing mode can be described by specifying β as a function of ϕ, with period ϕ_0. The transformation clearly depends on the size of the ''mismatch,'' that is, on the relative amplitude of the breathing oscillation. For completeness, we write the differential equation for $\beta(\phi)$:

$$\frac{\ddot{\beta}}{2\beta}=1+\frac{\beta I}{\epsilon}-k^2\beta^2+\frac{3}{4}\frac{\dot{\beta}^2}{\beta^2}. \tag{2.9}$$

If we scale β so that

$$\beta(\phi)=\sigma(\phi)/k \tag{2.10}$$

and define

$$\alpha=I/k\epsilon, \tag{2.11}$$

Eq. (2.9) can be written in terms of the single parameter α as

$$\frac{\ddot{\sigma}}{2\sigma}=1+\alpha\sigma-\sigma^2+\frac{3}{4}\frac{\dot{\sigma}^2}{\sigma^2}. \tag{2.12}$$

In terms of α and σ, the period of the breathing motion (in the variables z and ϕ) can be written as

$$kS=\int_{\sigma_1}^{\sigma_2}\frac{d\sigma}{\sigma^{1/2}p(\sigma)},\quad \phi_0=\int_{\sigma_1}^{\sigma_2}\frac{d\sigma}{\sigma^{3/2}p(\sigma)}, \tag{2.13}$$

where

$$p(\sigma)=\left[\alpha\ \ln\frac{\sigma}{\sigma_1}+\sigma_1-\sigma+\frac{1}{\sigma_1}-\frac{1}{\sigma}\right]^{1/2},$$

$$\sigma_1=\frac{k}{\epsilon}a_1^2. \tag{2.14}$$

Finally, we note that a matched beam (zero breathing amplitude) has the matched amplitude

$$\sigma_0=\frac{\alpha}{2}+\sqrt{1+\frac{\alpha^2}{4}} \tag{2.15}$$

and that the tune depression for a matched beam is given by

$$\eta\equiv\frac{(k^2-I/a_0^2)^{1/2}}{k}=\frac{1}{\sigma_0}=\sqrt{1+\frac{\alpha^2}{4}}-\frac{\alpha}{2}. \tag{2.16}$$

III. PHASE-SPACE DISTRIBUTION

We now wish to consider small perturbations from a uniform charge density breathing mode in the phase-space distribution. For this purpose, we use the variables $u(\phi)$, $v(\phi)$, and ϕ and write

$$f(u,v,\dot{u},\dot{v},\phi)=f_0(u,v,\dot{u},\dot{v})+f_1(u,v,\dot{u},\dot{v},\phi), \tag{3.1}$$

where the ''unperturbed'' distribution (including the breathing mode) is

$$f_0(u,v,\dot{u},\dot{v})=(\tau_0/\pi^2)\,\delta(u^2+v^2+\dot{u}^2+\dot{v}^2-1). \tag{3.2}$$

Here $\tau_0=I_0/v_0$ is the line charge density of the beam. In terms of the new variables, the Vlasov equation can be written as

$$\frac{\partial f}{\partial\phi}=-\dot{u}\frac{\partial f}{\partial u}-\dot{v}\frac{\partial f}{\partial v}-\ddot{u}\frac{\partial f}{\partial\dot{u}}-\ddot{v}\frac{\partial f}{\partial\dot{v}}. \tag{3.3}$$

The unperturbed distribution is clearly a solution of Eq. (3.3) if one uses Eq. (2.8), the unperturbed equation of motion.

We now write the charge density (in x,y space) as

$$\rho_0+\rho_1=\frac{1}{\beta\epsilon}\int d\dot{u}\int d\dot{v}[f_0+f_1]. \tag{3.4}$$

This leads to

$$\rho_0=\frac{I_0}{\pi v_0\beta\epsilon}\times\begin{cases}1, & u^2+v^2<1\\ 0, & u^2+v^2>1\end{cases} \tag{3.5}$$

and

$$\rho_1=\frac{1}{\beta\epsilon}\int d\dot{u}\int d\dot{v}\ \ f_1(u,v,\dot{u},\dot{v},\phi). \tag{3.6}$$

We assume that the electric field due to ρ_1 is derivable from a scalar potential $G(u,v,\phi)$ such that

$$E_x^{(1)} = -\frac{\partial G}{\sqrt{\beta\epsilon}\partial u}, \quad E_y^{(1)} = -\frac{\partial G}{\sqrt{\beta\epsilon}\partial v}, \tag{3.7}$$

and

$$\nabla\cdot\mathbf{E}_\perp = \frac{1}{\sqrt{\beta\epsilon}}\left(\frac{\partial E_x}{\partial u}+\frac{\partial E_y}{\partial v}\right) = \frac{\rho_1}{\epsilon_0} = -\frac{1}{\beta\epsilon}\left(\frac{\partial^2 G}{\partial u^2}+\frac{\partial^2 G}{\partial v^2}\right)$$
$$= \frac{1}{\beta\epsilon\epsilon_0}\int d\dot{u}\int d\dot{v} f_1. \tag{3.8}$$

The equations of motion, including the force due to the nonuniform charge distribution, are

$$\ddot{u}+u = -\frac{e}{Mv_0^2}\frac{\beta}{\epsilon}\frac{\partial G}{\partial u}, \quad \ddot{v}+v = -\frac{e}{Mv_0^2}\frac{\beta}{\epsilon}\frac{\partial G}{\partial v}. \tag{3.9}$$

Keeping only terms linear in f_1 or ρ_1 (or G), Eq. (3.3) becomes

$$\frac{\partial f_1}{\partial\phi}+\dot{u}\frac{\partial f_1}{\partial u}+\dot{v}\frac{\partial f_1}{\partial v}-u\frac{\partial f_1}{\partial\dot{u}}-v\frac{\partial f_1}{\partial\dot{v}}$$
$$= \frac{e}{Mv_0^2}\frac{\beta}{\epsilon}\left[\frac{\partial f_0}{\partial\dot{u}}\frac{\partial G}{\partial u}+\frac{\partial f_0}{\partial\dot{v}}\frac{\partial G}{\partial v}\right]. \tag{3.10}$$

Since f_0 is a function of $u^2+v^2+\dot{u}^2+\dot{v}^2$, as in Eq. (3.2), we can write

$$\frac{\partial f_0}{\partial\dot{u}} = 2\dot{u}f_0', \quad \frac{\partial f_0}{\partial\dot{v}} = 2\dot{v}f_0'. \tag{3.11}$$

If we now write

$$f_1(u,v,\dot{u},\dot{v},\phi) = g(u,v,\dot{u},\dot{v},\phi)f_0'(u^2+v^2+\dot{u}^2+\dot{v}^2), \tag{3.12}$$

all operations on f_0' on the left-hand side of Eq. (3.10) will cancel, leaving

$$\frac{\partial g}{\partial\phi}+\dot{u}\frac{\partial g}{\partial u}+\dot{v}\frac{\partial g}{\partial v}-u\frac{\partial g}{\partial\dot{u}}-v\frac{\partial g}{\partial\dot{v}} = R(u,v,\dot{u},\dot{v},\phi), \tag{3.13}$$

where the right-hand side is

$$R(u,v,\dot{u},\dot{v},\phi) = \frac{2e}{Mv_0^2}\frac{\beta}{\epsilon}\left[\dot{u}\frac{\partial G}{\partial u}+\dot{v}\frac{\partial G}{\partial v}\right]. \tag{3.14}$$

Equations (3.8) and (3.13) are coupled integro-differential equations. Since the operator on the left-hand side of Eq. (3.13) corresponds to the sinusoidal orbits in Eq. (2.8), Eq. (3.13) has a formal solution, which can be written as

$$g(u,v,\dot{u},\dot{v},\phi) = \int_{-\infty}^{\phi} d\psi R(u',v',\dot{u}',\dot{v}',\psi), \tag{3.15}$$

where

$$u' = uc-\dot{u}s, \quad v' = vc-\dot{v}s,$$
$$\dot{u}' = \dot{u}c+us, \quad \dot{v}' = \dot{v}c+vs, \tag{3.16}$$

with

$$c\equiv\cos(\phi-\psi), \quad s\equiv\sin(\phi-\psi). \tag{3.17}$$

We now proceed, as in the analysis for a matched KV beam [7], to guess at the form of the potential $G(u,v,\phi)$ and to determine the perturbed phase-space distribution $g(u,v,\dot{u},\dot{v},\phi)$ using Eq. (3.15). Using Eqs. (3.12) and (3.8), we then obtain $\partial^2G/\partial u^2+\partial^2G/\partial v^2$ and require that it agree with our guess for G. Remarkably, our guess, which is almost identical to the form used for the matched KV beam, works once again.

We now conjecture that $G(u,v,\phi)$ is

$$G(u,v,\phi) = P(\phi)F(u,v), \tag{3.18}$$

with

$$F(u,v) = (u+iv)^m{}_2F_1(-j,m+j;m+1;u^2+v^2)$$
$$= d_{jm}\sum_l \frac{i^{2l}(m+j+l-1)!}{l!(m+l)!(j-l)!}(u+iv)^{l+m}(u-iv)^l, \tag{3.19}$$

where $d_{jm} = j!m!/(m+j-1)!$, and show in the Appendix that Eqs. (3.8) and (3.13) can both be satisfied as long as $P(\phi)$ satisfies the integral equation

$$P(\phi) = -\alpha\int_{-\infty}^{\phi} d\psi P(\psi)\sigma(\psi)\frac{\partial Q}{\partial\psi}, \tag{3.20}$$

where

$$Q(\phi-\psi) = (-1)^j\sum_r \frac{(-1)^r(m+j+r-1)!}{r!(m+r)!(j-r)!}\cos^{m+2r}(\phi-\psi)$$
$$= (-1)^j[d_{jm}]^{-1}\cos^m(\phi-\psi)$$
$$\times{}_2F_1(-j,m+j;m+1;\cos^2(\phi-\psi)) \tag{3.21}$$

and $\sigma(\phi)$ and α are defined in Eqs. (2.10) and (2.11). To recapitulate, we have confirmed that the conjecture for the electrostatic potential in Eq. (3.18) leads to a perturbed phase space density in Eq. (3.12) that reproduces the perturbed space-charge density corresponding to the potential in Eq. (3.18), provided $P(\phi)$ satisfies the integral equation in Eq. (3.20).

IV. DIFFERENTIAL EQUATION FOR $P(\phi)$

The integral equation for $P(\phi)$ in Eq. (3.20) can be converted to a linear differential equation with periodic coefficients. As an illustration, we consider the case $j=2$, $m=0$, for which

$$Q(\phi-\psi) = \frac{1}{2}-2\cos^2(\phi-\psi)+\frac{3}{2}\cos^4(\phi-\psi) \tag{4.1}$$

and

$$\frac{\partial Q}{\partial \psi} = -4\ \sin(\phi-\psi)\cos(\phi-\psi) + 6\ \sin(\phi-\psi)\cos^3(\phi-\psi)$$

$$= -\frac{\sin 2(\phi-\psi)}{2} + \frac{3\ \sin 4(\phi-\psi)}{4}. \tag{4.2}$$

Equation (3.20) can then be written as

$$P(\phi) = \alpha \int_{-\infty}^{\phi} d\psi P(\psi)\sigma(\psi)\left[\frac{\sin 2(\phi-\psi)}{2} - \frac{3\sin 4(\phi-\psi)}{4}\right]. \tag{4.3}$$

We now take successive derivatives of Eq. (4.3) with respect to ϕ, obtaining contributions from both the upper limit of the integral and the integrand. Specifically,

$$\dot{P}(\phi) = \alpha \int_{-\infty}^{\phi} d\psi P(\psi)\sigma(\psi)[\cos 2(\phi-\psi) - 3\cos 4(\phi-\psi)], \tag{4.4}$$

$$\ddot{P}(\phi) = -2\alpha P(\phi)\sigma(\phi) + \alpha \int_{-\infty}^{\phi} d\psi P(\psi)\sigma(\psi) \times[-2\sin 2(\phi-\psi) + 12\ \sin 4(\phi-\psi)], \tag{4.5}$$

$$\dddot{P}(\phi) = -2\alpha[\dot{P}(\phi)\sigma(\phi) + P(\phi)\dot{\sigma}(\phi)] + \alpha \int_{-\infty}^{\phi} d\psi P(\psi)\sigma(\psi)[-4\ \cos 2(\phi-\psi) + 48\ \sin 4(\phi-\psi)], \tag{4.6}$$

$$P^{iv}(\phi) = -2\alpha[\ddot{P}(\phi)\sigma(\phi) + 2\dot{P}(\phi)\dot{\sigma}(\phi) + P(\phi)\ddot{\sigma}(\phi)] + 44\alpha P(\phi)\sigma(\phi) + \alpha \int_{-\infty}^{\phi} d\psi P(\psi)\sigma(\psi) \times[8\sin 2(\phi-\psi) - 192\ \sin 4(\phi-\psi)]. \tag{4.7}$$

It now is possible to construct a linear combination of Eqs. (4.3), (4.5), and (4.7) in which the integrals cancel. Specifically

$$P^{iv} + 20\ddot{P} + 64P = -2\alpha[\ddot{P}\sigma + 2\dot{P}\dot{\sigma} + P\ddot{\sigma}] + 4\alpha P\sigma \tag{4.8}$$

or

$$P^{iv} + (20 + 2\alpha\sigma)\ddot{P} + 4\alpha\dot{\sigma}\dot{P} + (64 - 4\alpha\sigma + 2\alpha\ddot{\sigma})P = 0. \tag{4.9}$$

Since $\sigma(\phi)$ in Eq. (2.12) is a periodic function of ϕ with period ϕ_0, Eq. (4.9) is a Mathieu-like equation for $P(\phi)$.

We now define

$$\dot{P} \equiv L, \quad \dot{L} \equiv K, \quad \dot{K} \equiv H \tag{4.10}$$

and let V be the four-component vector (P,L,K,H). Equations (4.9) and (4.10) can then be written as the single 4×4 matrix equation

$$\dot{V} = TV, \tag{4.11}$$

where the matrix T depends on ϕ because σ depends on ϕ, and has the explicit form

$$T(\phi) = \begin{pmatrix} 0 & 1 & 0 & 0 \\ 0 & 0 & 1 & 0 \\ 0 & 0 & 0 & 1 \\ -64 + 4\alpha\sigma - 2\alpha\ddot{\sigma} & -4\alpha\dot{\sigma} & -20 - 2\alpha\sigma & 0 \end{pmatrix}. \tag{4.12}$$

If one divides the breathing period into small intervals $d\phi_l$, the matrix corresponding to one period can be written as the (infinite) product

$$\mathcal{T} = \prod_l\ [1 + T(\phi_l)d\phi_l]. \tag{4.13}$$

Diagonalization of $\mathcal{T}$ then determines the stability of the mode denoted by j,m for the space charge α and the mismatch contained in $\sigma(\phi)$. Specifically, the mode will be unstable if the absolute value of any of the eigenvalues of $\mathcal{T}$ is greater than 1.

For general j and m, $\partial Q/\partial\psi$ can be written as the sum of $j+m/2$ or $j+(m+1)/2$ terms in the form

$$\frac{\partial Q}{\partial \psi} = \sum_{r=0}\ \gamma_r \sin(2j+m-2r)\phi. \tag{4.14}$$

By taking $2j+m$ or $2j+m+1$ derivatives of $P(\phi)$, it is always possible to construct a linear combination that eliminates all the integrals, as we did in Eq. (4.8). The order of the resulting differential equation is $2j+m$ for m even or $2j+m+1$ for m odd, as is also the dimension of the vector V and the square matrix $\mathcal{T}$.

V. NUMERICAL STUDIES

To determine the stability of a particular mode of density oscillation, we first solve Eq. (2.12) for the envelope oscillation numerically and substitute the values of σ, $\dot{\sigma}$, and $\ddot{\sigma}$ for a breathing period into the product of Eq. (4.13). The eigenvalues of the transfer matrix $\mathcal{T}$ for a breathing period can then be obtained for various values of the parameters α and σ_1. The numerical calculations show that, for small tune depression, the results for the eigenvalue converge rapidly as the number of subintervals reaches 1000. Since lower space charge gives a larger breathing period [cf. Eqs. (2.13) and (2.14)], the number of steps to complete the matrix product needs to be increased by making $d\phi_l$ small in order to achieve the required accuracy as the tune depression increases. Another way to improve accuracy is to use the Runge-Kutta method. By assuming that the initial condition of the ith component of the vector V is 1, and zero elsewhere, the ith column of the one-turn map $\mathcal{T}$ can thus be obtained from the solutions of V at the final point of one period. The eigenvalue spectrum is then obtained after the construction of the whole map.

If we use a fourth-order Runge-Kutta algorithm for large tune depression, the number of steps needed to achieve the required accuracy is much smaller than with the matrix product. However, since a larger initial mismatch causes a larger

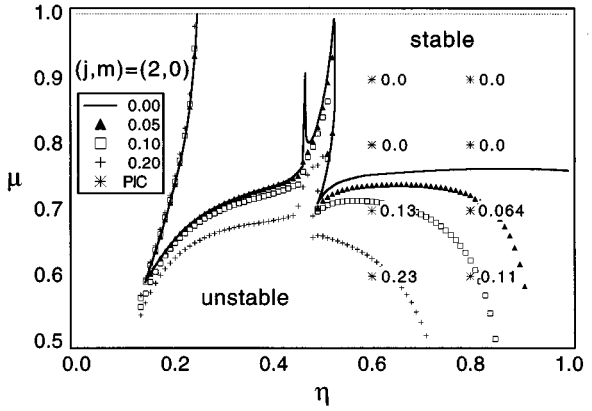

FIG. 1. Stability limits and growth rates for the $j=2,m=0$ mode in the mismatch (μ) tune depression (η) space. Contours for growth rates of 0.05, 0.10, and 0.20 are shown, as well as growth rates obtained from particle-in-cell (PIC) simulations.

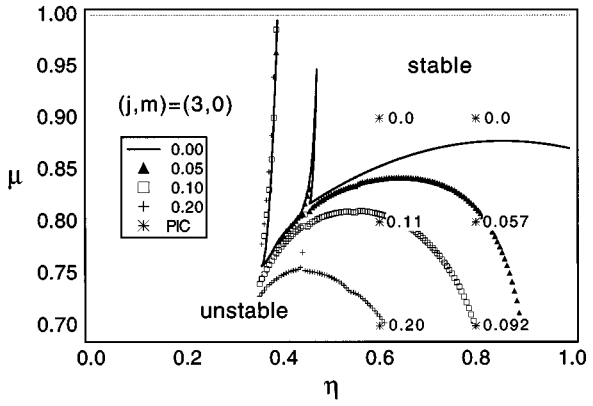

FIG. 2. Same as in Fig. 1, but for the $j=3,m=0$ mode.

and sharper amplitude of envelope oscillation, the numerical integration scheme needs more steps to yield sufficiently accurate results. Therefore, for high space charge, we use the matrix product that is much faster than the Runge-Kutta method and gives accurate results. For low space charge, the situation is just the opposite. The two methods nevertheless give convergent results with differences less than 10 ppm.

Starting with the integral equation for $P(\phi)$ in Eq. (3.20) and making the transformation in a fashion similar to that shown in Sec. IV, we obtain differential equations for $P_{30}(\phi)$ and $P_{40}(\phi)$ similar to the one in Eq. (4.9) for $P_{20}(\phi)$. In the case of a matched beam ($\sigma=\sigma_0=$constant) $P_{jm}(\phi)$ takes on the sinusoidal form $\exp(i\lambda_{jm}\phi)$. In this case the eigenvalues λ_{20}, λ_{30}, and λ_{40} satisfy the equations

$$(\lambda_{20}^2-16)(\lambda_{20}^2-4)=2\alpha\sigma_0(\lambda_{20}^2+2), \tag{5.1}$$

$$(\lambda_{30}^2-36)(\lambda_{30}^2-16)(\lambda_{30}^2-4)=2\alpha\sigma_0(\lambda_{30}^4-4\lambda_{30}^2+48), \tag{5.2}$$

$$(\lambda_{40}^2-64)(\lambda_{40}^2-36)(\lambda_{40}^2-16)(\lambda_{40}^2-4) =2\alpha\sigma_0(\lambda_{40}^6-26\lambda_{40}^4+304\lambda_{40}^2+1296). \tag{5.3}$$

Note that the breathing mode $(\lambda_{10}^2-4)=2\alpha\sigma_0$ is always stable and the matched beam's stability limits of the modes $(j,m)=(2,0),(3,0)$, and (4,0) are where $\eta_{\rm limit}=0.2425$, 0.3859, and 0.3985, respectively. In fact, $m=0$ is the most restrictive mode for all m and $j=4$ is the most serious mode that gives the largest threshold value of η, i.e., the smallest space-charge limit, for all $(j,0)$ modes [8]. Therefore, the (4,0) mode is the least stable mode for the space-charge limit of a KV beam. In Figs. 1–3 we show the stability diagram for these three cases in μ-η space, where $\mu\equiv a_1/a_0$. The value of $\eta_{\rm limit}$ on the $\mu=1$ axis for each case is confirmed in the figures.

The cusps appearing in these stability diagrams are caused by the resonances of the mode frequency. In Fig. 1, the deep fissure up to the matched parameter $\mu=1$ is where the phase advance of the (2,0) mode oscillation during one period of the breathing mode is π. Note that this resonance is where the ratio of the breathing frequency to the mode frequency is equal to 2. It is believed that the other slits appearing in the stable domains are also due to the occurrence of resonances for particular parameters of tune depression and mismatch. As for the higher modes (3,0) and (4,0), the $\phi=\pi$ resonance occurs outside of their stability limits. That is why the deep fissure that meets the $\mu=1$ axis is not seen in either Fig. 2 or 3. One can also see that as the number of the radial mode j is higher, not only does the stability limit of η move ''backward,'' i.e., to smaller space charge, but also the stable bandwidth for the mismatch parameter μ becomes narrower. This implies that, at least up to $j=4$ for a KV beam, the area of stability decreases as j increases. We have obtained also some results on the stability of even higher modes $j=5$ and $j=6$ mostly from direct multiparticle simulations described below. Based on these results, one can conclude that their stability boundaries are close to that for the mode $j=4$. However, since both the numerical analysis and the mode amplitude extraction from simulations are rather involved for these high-order modes, we have not yet carried out the detailed study.

Our numerical procedure in obtaining the eigenvalues of $\mathcal{T}$ also provides the growth rate per breathing period in the unstable region as a function of μ and η. In Figs. 1–3 we also show the contours corresponding to growth rates of 5%, 10%, and 20%. The values for $\mu=1$ agree with those obtained earlier [8,9], which predicted instability for tune depressions below 0.4. The present predictions are dramati-

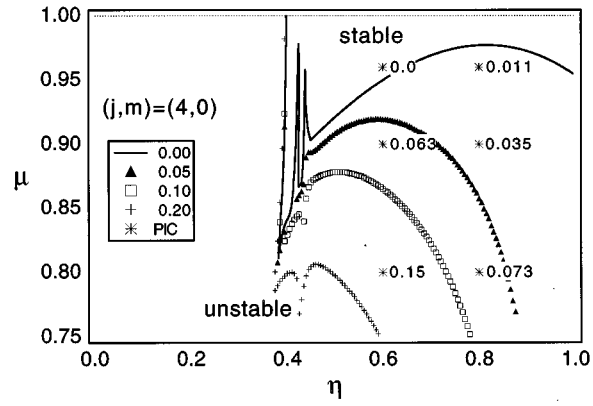

FIG. 3. Same as in Fig. 1, but for the $j=4,m=0$ mode.

cally different: instabilities are possible for almost all tune depressions if the mismatch is sufficient.

VI. MULTIPARTICLE SIMULATIONS

We have also performed multiparticle simulations for an azimuthally symmetric breathing KV beam. For $m=0$ it is easy to show that the charge density of the mode (j,m) is proportional to

$$\rho_{j0}(w)\sim-\nabla^2 G_{j0}(w)=4j^2 G_{j0}(w)/(1-w^2). \quad (6.1)$$

The orthogonality relation for the hypergeometric function ${}_2F_1$ then yields

$$\int_0^1 w\, dw\, \rho_{j0}(w)\rho_{j'0}(w)(1-w^2)=\delta_{jj'}/4j, \quad (6.2)$$

which can be used to project out each value of j from the numerical results for the charge distribution. Using this procedure, we start with the order of 10^5 particles distributed in phase space according to Eq. (3.1) for a particular mismatch μ and depressed tune η. All unstable modes will start to grow from the noise. By projecting out the amplitude of the jth mode charge density we can determine whether it is unstable and, if so, what its growth rate is. It is of course necessary to examine the growth at low amplitude since the phase-space density of the core will be altered when the unstable modes become too large.

This procedure was followed for several different values of μ and η using $j=2,3,4$. The results are shown on Figs. 1–3 as specific points for which the growth rates are measured. As can be seen, the growth rates obtained in the multiparticle simulations agree closely with those predicted from the matrix eigenvalues.

The particle-in-cell simulations are also used to study halo formation in the presence of instabilities, as a function of tune depression η and mismatch μ. We load a mismatched initial KV distribution choosing $r_i=\mu\tilde{r}_i$, $r_i'=\tilde{r}_i'/\mu$, where $\tilde{r}_i,\tilde{r}_i'$ correspond to the matched distribution, and use leapfrog integration to track the particles. A typical range of the simulation parameters is as follows: time step $\Delta t=T/100$, where T is the period of breathing oscillations; total number of particles $N_{\rm par}=16K$–$4096K$, where $K=1024$; and radial mesh size $\Delta r=a/128$–$a/16$. In simulations we use dimensionless variables normalized in such a way that $a'_{\rm max}a_{\rm min}=1$ and matched radius $a=1/\sqrt{\eta}$.

The beam evolution depends on the values of η and μ. If we look at the maximal radius $r_{\rm max}$ of the whole ensemble of particles, a rather typical picture of the beam behavior is shown in Fig. 4 for the particular case of $\eta=0.7$ and $\mu=0.8$: after a number of breathing oscillations a fast growth of $r_{\rm max}$ occurs, after which the maximal radius shows more or less stable oscillations around a new level, which is usually more than twice the initial one. The beam distribution in the transverse phase space r,r' after that moment clearly shows the presence of the beam halo; see Fig. 5. This figure is a stroboscopic phase-space plot for a small sample of particles with low angular momenta. The number of particles that escape from the beam core to larger radii and thus form the halo is counted at each integration step. We define

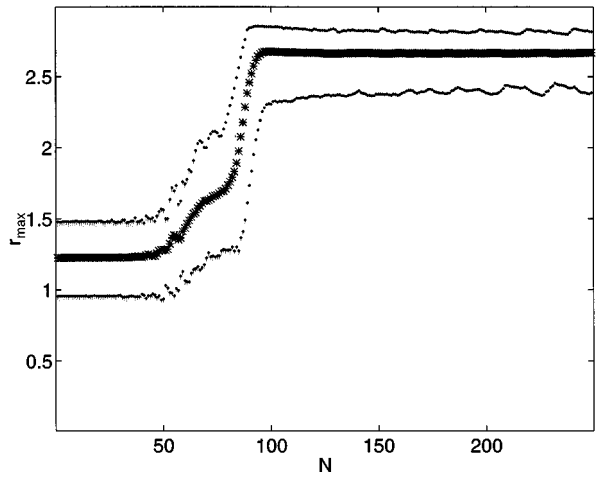

FIG. 4. Maximal beam radius versus the number of breathing oscillations for $\eta=0.7$ and $\mu=0.8$. Stars are for the average over the period, dots show the minimal and maximal values.

the halo intensity h as the number of particles outside the boundary $r_b=1.75a$ divided by the total number of particles in the beam. While such a definition looks rather arbitrary, it is convenient to compare beam halos in the wide range on the tune depressions. The evolution of the halo intensity is shown in Fig. 6 for the same parameters as in Figs. 4 and 5.

Exploring the KV beam behavior for various values of the tune depression and mismatch reveals the picture shown in Fig. 7. The marks on the (η,μ) plane have the following meaning: H corresponds to beam instability with halo formation and usually with a noticeable growth of the beam rms emittance, U means that the beam is unstable, but a halo is not observed, at least at the level detectable in simulations done, and S indicates beam stability. One can see that even the matched KV beam is unstable for tune depression $\eta\leqslant 0.4$, in agreement with the existing theory [7] and earlier simulations [8]. The most intriguing feature of the diagram shown is the lack of any essential dependence on η for mismatched beams. On the contrary, the qualitative changes de-

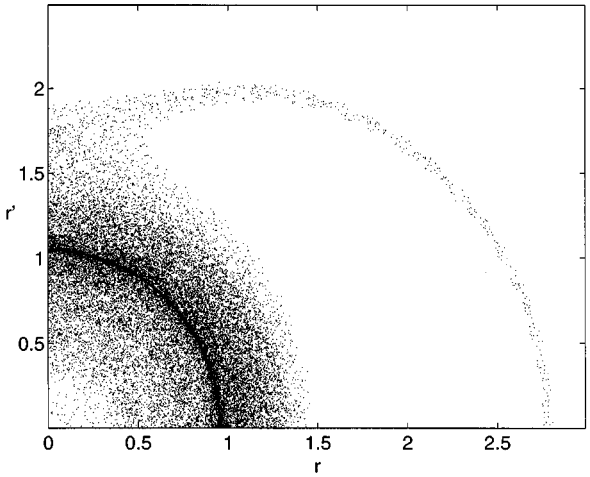

FIG. 5. Stroboscopic plot in the transverse phase space for 125 particles with low angular momenta. The dark elliptic arc corresponds to the initial distribution ($\eta=0.7$, $\mu=0.8$).

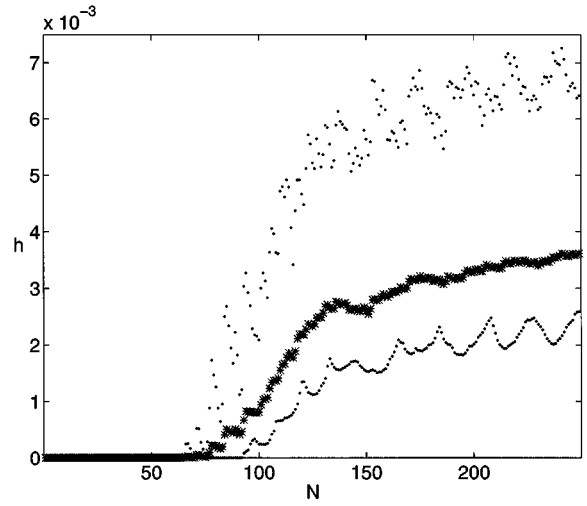

FIG. 6. Halo intensity vs the number of breathing oscillations. Stars are for the average over the period, dots show the minimal and maximal values ($\eta=0.7$, $\mu=0.8$).

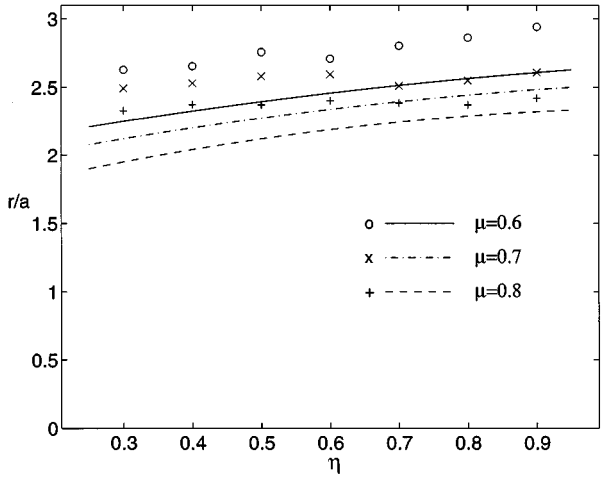

FIG. 8. Ratio of halo radius to the matched beam radius vs tune depression η for mismatch $\mu=0.6,0.7,0.8$. Curves show predictions of the analytical model.

pend primarily on μ. Thus, when μ changes from 0.6 to 0.8, the ratio of the final beam rms emittance to the initial one decreases from 1.7–2 to 1.03–1.07. There is some dependence on η of the number of breathing periods after which the beam radius starts to grow noticeably and the halo forms. For example, with the 40% mismatch $\mu=0.6$, it takes 10–20 periods for the beam to reach its maximal size for $\eta=0.3$, while for $\eta=0.9$ the same occurs in 50–90 periods. This is related to the fact that the growth rates of the unstable modes are larger for smaller values of the tune depression η, as seen in Figs. 1–3.

To make a comparison with predictions of the analytical model of halo formation via the parametric resonance with breathing oscillations [6], the ratio of the halo radius to the matched beam radius is plotted in Fig. 8. One can see that this ratio is almost independent of the tune depression for a given mismatch and slightly lower for smaller mismatches. For $\mu=0.8$ there is better agreement with the analytical model, as it should be, since the latter is applicable for small mismatches. Since the beam matched radius $a\propto 1/\sqrt{\eta}$, the same scaling law holds for the halo radius.

The halo intensity h defined above is shown in Fig. 9 as a function of tune depression and mismatch. It can be as large as a few percent for mismatch $\mu=0.6$ and decreases an order of magnitude as the mismatch decreases from 40% to 20% for a given tune. As for an apparent decrease of h as η decreases for a fixed mismatch, it is due to the definition used: we count particles in the halo with $r>1.75a$, so that the boundary radius increases as $1/\sqrt{\eta}$. If we use instead a fixed boundary, the same for all tunes, the halo intensity would be larger for larger space charge.

VII. SUMMARY AND CONCLUSIONS

We have analyzed the stability of a breathing KV beam by constructing the eigenmodes for charge-density fluctuations. For these we determined the stability limits for the $m=0$, $j=2,3,4$ modes in the mismatch (μ) tune depression (η) space as well as the growth rates per breathing period when the mode is unstable. We then used a multiparticle simulation to confirm both the stability limit and the growth rates.

These calculations show clearly that a breathing beam is much more likely to be unstable than a perfectly matched

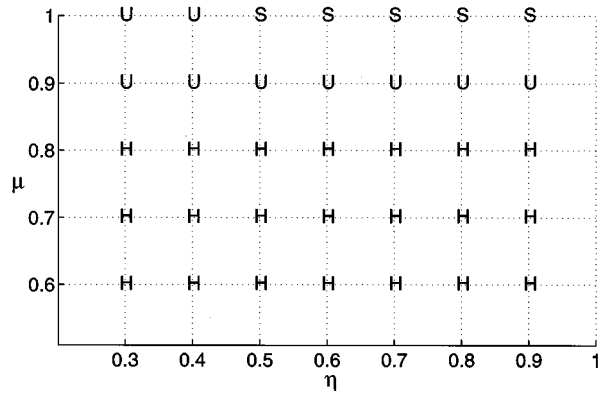

FIG. 7. Beam behavior vs tune depression η and mismatch μ (see the text for the legend).

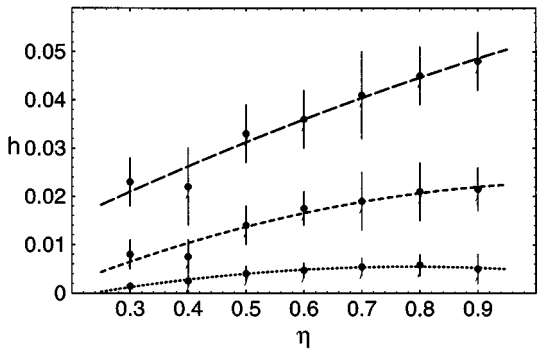

FIG. 9. Halo intensity vs tune depression η: long-dashed line, $\mu=0.6$; short-dashed line, $\mu=0.7$; and dotted line, $\mu=0.8$. Points with error bars are from simulations, curves fit the data.

beam. For example, with a matched beam, the $j=4$ mode is stable as long as the tune depression is not below $\eta=0.4$, while with a mismatch parameter $\mu=0.9$ ($\sim$10% mismatch) the $j=4$ mode is unstable even at $\eta=0.8$. At the same time, the growth rates are much smaller at higher values of η. In fact, multiparticle simulations indicate that the instabilities are highly nonlinear and appear to saturate without excessive growth.

The simulations reveal also that stability of a mismatched KV beam, as well as its halo intensity, depends primarily on the mismatch, not on the tune depression. The numerical results show, particularly, that the ratio of the halo radius to that of the matched beam is independent of η, and this agrees reasonably well with predictions of the analytical model [6] for halo formation.

Though our analysis is valid only for a KV beam, we believe that similar instabilities will be present in other equilibrium beam distributions when they perform collective oscillations such as breathing. We plan to examine multiparticle simulations for other phase-space distributions such as the waterbag.

The implication of the above conclusions is clear. Every effort must be made to minimize beam mismatch, particularly when transitions in the beam channel occur. In addition, designs should use modest values of the tune depression. In this way we may be able to minimize or avoid the presence of beam instabilities, which are likely to lead to halo formation.

ACKNOWLEDGMENTS

The authors wish to acknowledge support from the U.S. Department of Energy. They are also grateful to Dr. Irving Haber (NRL) and Dr. Robert Ryne (LANL) for helpful discussions and for guidance with regard to the particle-in-cell simulation.

APPENDIX

In this appendix we show that the conjecture in Eqs. (3.18) and (3.19) correctly satisfies Eqs. (3.8) and (3.13). Here $P(\phi)$ is a function periodic in ϕ (with period ϕ_0, the same as that of the breathing oscillation), which is to be determined. The corresponding charge density, according to Eq. (3.8), is

$$\begin{aligned}\rho_1(u,v,\phi)&=-\frac{4\epsilon_0}{\epsilon}\frac{P(\phi)}{\beta(\phi)}d_{jm}\sum_l\frac{(-1)^l(m+j+l-1)!}{(l-1)!(m+l-1)!(j-l)!}\\&\quad(u+iv)^{l+m-1}(u-iv)^{l-1}\\&=\frac{4\epsilon_0}{\epsilon}\frac{P(\phi)}{\beta(\phi)}d_{jm}\sum_l\frac{(-1)^l(m+j+l)!}{l!(m+l)!(j-1-l)!}\\&\quad\times(u+iv)^{l+m}(u-iv)^l,\end{aligned}\tag{A1}$$

with m and $j-1$ being the number of azimuthal and radial nodes in the perturbed charge density.

From Eq. (3.16), we have $\partial u'/\partial\psi=\dot{u}'$ and $\partial v'/\partial\psi=\dot{v}'$. We therefore can write Eq. (3.14) as

$$R(u',v',\dot{u}',\dot{v}',\psi)=\frac{2e}{Mv_0^2}\frac{\beta(\psi)}{\epsilon}P(\psi)\frac{\partial F(u',v')}{\partial\psi}\tag{A2}$$

and obtain g from Eq. (3.15) as

$$g(u',v',\dot{u}',\dot{v}',\phi)=\frac{2e}{Mv_0^2\epsilon}\int_{-\infty}^{\phi}d\psi P(\psi)\beta(\psi)\frac{\partial F}{\partial\psi}(u',v').\tag{A3}$$

We now write

$$u\pm iv\equiv we^{\pm i\theta},\quad \dot{u}+i\dot{v}=\zeta e^{\pm i\chi},\tag{A4}$$

and from Eq. (3.16) find that

$$u'\pm iv'=wce^{\pm i\theta}-\zeta se^{\pm i\chi}.\tag{A5}$$

From Eqs. (3.2), (3.8), and (3.12) we then can write

$$\begin{aligned}\rho_1&=\frac{\tau_0}{\pi^2\beta\epsilon}\int\int\zeta\ d\zeta\ d\chi\ g(w,\theta,\zeta,\chi)\delta'(w^2+\zeta^2-1)\\&=-\frac{\tau_0}{\pi\beta\epsilon}\frac{\partial}{\partial\zeta^2}\langle g\rangle_\chi|_{\zeta^2=1-w^2},\end{aligned}\tag{A6}$$

where $\langle\ \rangle_\chi$ stands for the average over χ. From Eq. (A3)

$$\langle g\rangle_\chi=\frac{2e}{Mv_0^2\epsilon}\int_{-\infty}^{\phi}d\psi P(\psi)\beta(\psi)\frac{\partial}{\partial\psi}\langle F(u',v')\rangle_\chi.\tag{A7}$$

Using Eq. (3.19),

$$\begin{aligned}\langle F(u',v')\rangle_\chi&=d_{jm}\sum_l\frac{(-1)^l(m+j+l-1)!}{l!(m+l)!(j-l)!}\\&\quad\times\langle(wce^{i\theta}-\zeta se^{i\chi})^{l+m}\\&\quad\times(wce^{-i\theta}-\zeta se^{-i\chi})^l\rangle_\chi.\end{aligned}\tag{A8}$$

We now expand the two factors within $\langle\rangle_\chi$ in powers of $\zeta se^{\pm i\chi}$. The average over χ vanishes unless the power of $\zeta se^{\pm i\chi}$ is the same in each factor. Thus

$$\langle F(u',v')\rangle_\chi = d_{jm}e^{im\theta}\times\sum_l\sum_p \frac{(-1)^l(m+j+l-1)!(wc)^{2l+m-2p}\zeta^{2p}s^{2p}}{(l-p)!(m+l-p)!(j-l)!p!p!}. \tag{A9}$$

Guided by Eq. (A6) we find

$$\frac{\partial}{\partial\zeta^2}\langle F\rangle_\chi\big|_{\zeta^2=1-w^2} = d_{jm}w^m e^{im\theta}c^m\sum_l \frac{(-1)^l(m+j+l-1)!}{(j-l)!} \times\sum_p \frac{1}{(m+l-p)!(l-p)!}\sum_q\sum_r \times\frac{w^{2q}c^{2r}(-1)^{q+r}}{(q-l+p)!(l-q-1)!(r-l+p)!(l-r)!}, \tag{A10}$$

where we have collected the exponents of w and c to obtain $w^{2q}c^{2r}$ by using

$$\zeta^{2p-2}=(1-w^2)^{p-1} =\sum_q \frac{(-1)^{q-l+p}(p-1)!}{(q-l+p)!(l-q-1)!}w^{2q-2\not{\ell}+2p} \tag{A11}$$

and

$$s^{2p}=(1-c^2)^p=\sum_r \frac{(-1)^{r-l+p}p!}{(r-l+p)!(l-r)!}c^{2r-2l+2p}. \tag{A12}$$

The sum over p in Eq. (A10) can now be performed [10] using

$$\sum_p \frac{1}{(A+p)!(B-p)!(C+p)!(D-p)!} =\frac{(A+B+C+D)!}{(A+B)!(C+D)!(A+D)!(B+C)!}. \tag{A13}$$

This makes it possible to do the sum over l, using

$$\sum_{\not{\ell}} \frac{(-1)^l(l+E)!}{(A+l)!(B-l)!(C+l)!} =\frac{(-1)^B(E-A)!(E-C)!}{(A+B)!(B+C)!(E-A-B-C)!}. \tag{A14}$$

Remarkably, this leads to the factorization of Eq. (A10) into the product of a factor depending on w and a factor depending on c. Specifically,

$$\frac{\partial}{\partial\zeta^2}\langle F\rangle_\chi\big|_{\zeta^2=1-w^2} = d_{jm}w^m e^{im\theta}(-1)^j\sum_q \frac{(-1)^q w^{2q}(m+j+q)!}{q!(m+q)!(j-q-1)!} \times\sum_r \frac{(-1)^r c^{2r+m}(m+j+r-1)!}{(m+r)!r!(j-r)!}, \tag{A15}$$

where the first factor closely resembles the second factor in Eq. (3.19), using $u\pm iv=we^{\pm i\theta}$ and $l\to q$. Using Eqs. (3.19), (A6), and (A7) and canceling the factor depending on w on each side of the equation, we finally obtain an integral equation for $P(\phi)$,

$$P(\phi)=-\alpha\int d\psi P(\psi)\sigma(\psi)\frac{\partial Q}{\partial\psi}, \tag{A16}$$

where $Q(\phi-\psi)$ satisfies Eq. (3.21).

[1] R.A. Jameson, Los Alamos Report No. LA-UR-93-1209, 1993 (unpublished). In this report Jameson describes the early observations of emittance growth and halo production, with particular reference to unpublished simulations and observations by R. A. Jameson, R. S. Mills, and G. P. Boicourt.

[2] (a) M. Reiser, in *Emittance Growth in Mismatched Particle Beams*, Proceedings of the Particle Accelerator Conference, San Francisco, 1991, edited by Loretta Lizama (IEEE, New York, 1991), p. 2497; (b) A. Cucchetti, M. Reiser, and T. Wangler, in *Simulation Studies of Emittance Growth in RMS Mismatched Beams*, *ibid.*, p. 251; (c) D. Kehne, M. Reiser, and H. Rudd, in *Numerical and Experimental Studies of Halo Formation Due to Mismatch in a Space-Charge Dominated Electron Beam*, Proceedings of the Particle Accelerator Conference, Washington, DC, 1993, edited by Stephen Corneliassen (IEEE, New York, 1993), p. 65.

[3] J.S. O'Connell, T.P. Wangler, R.S. Mills, and K.R. Crandall, in *Beam Halo Formation from Space-Charge Dominated Beams in Uniform Focusing Channels* [Ref. [(c2)]], p. 3657.

[4] C. Chen and R.C. Davidson, Phys. Rev. Lett. **72**, 2195 (1994).

[5] J.M. Lagniel, Nucl. Instrum. Methods Phys. Res. Sect. A **345**, 46 (1994); **345**, 405 (1994).

[6] R.L. Gluckstern, Phys. Rev. Lett. **73**, 1247 (1994).

[7] R.L. Gluckstern, in *Proceedings of the Linac Conference, Fermilab, 1970*, edited by M. R. Tracy (National Accelerator Laboratory, Batavia, IL, 1970), p. 811.

[8] I. Hofmann, L.J. Laslett, L. Smith, and I. Haber, Part. Accel. **13**, 145 (1983).

[9] R.L. Gluckstern, W.-H. Cheng, and H. Ye, Phys. Rev. Lett. **75**, 2835 (1995).

[10] Equations (A13) and (A14) are examples of Saalschütz's formula [cf. *Higher Transcendental Functions* (McGraw-Hill, New York, 1953), p. 66, Eq. (30)]. They can be easily derived starting with the identity

$$\int_0^{2\pi} d\theta (1+e^{i\theta})^P (1+e^{-i\theta})^Q e^{-i\theta R} = \int_0^{2\pi} d\theta (1+e^{i\theta})^{P+Q} e^{-i\theta(Q+R)}$$

and using the binomial expansion for the factors in the integrands. In our applications, P, Q, and R are positive or negative integers.